HHS Public Access

Author manuscript

Adv Mater. Author manuscript; available in PMC 2018 January 01.

Published in final edited form as:

Adv Mater. 2017 January ; 29(3): . doi:10.1002/adma.201604630.

Rapid Continuous Multi-Material Extrusion Bioprinting

Wanjun Liu[†],
Biomaterials Innovation Research Center, Division of Engineering in Medicine, Brigham and Women's Hospital, Harvard Medical School, Cambridge, MA 02139, USA

Harvard-MIT Division of Health Sciences and Technology, Massachusetts Institute of Technology, Cambridge, MA 02139, USA

Key Laboratory of Textile Science and Technology, College of Textiles, Donghua University, Shanghai 201620, China

Dr. Yu Shrike Zhang[†],
Biomaterials Innovation Research Center, Division of Engineering in Medicine, Brigham and Women's Hospital, Harvard Medical School, Cambridge, MA 02139, USA

Harvard-MIT Division of Health Sciences and Technology, Massachusetts Institute of Technology, Cambridge, MA 02139, USA

Wyss Institute for Biologically Inspired Engineering, Harvard University, Boston, MA 02115, USA

Marcel A. Heinrich[†],
Biomaterials Innovation Research Center, Division of Engineering in Medicine, Brigham and Women's Hospital, Harvard Medical School, Cambridge, MA 02139, USA

Harvard-MIT Division of Health Sciences and Technology, Massachusetts Institute of Technology, Cambridge, MA 02139, USA

MIRA Institute of Biomedical Technology and Technical Medicine, Department of Developmental BioEngineering, University of Twente, Enschede 7500AE, Netherlands

Fabio De Ferrari,
Biomaterials Innovation Research Center, Division of Engineering in Medicine, Brigham and Women's Hospital, Harvard Medical School, Cambridge, MA 02139, USA

Harvard-MIT Division of Health Sciences and Technology, Massachusetts Institute of Technology, Cambridge, MA 02139, USA

Department of Electronics and Telecommunications, Politecnico di Torino, Torino 10129, Italy

Dr. Hae Lin Jang,
Biomaterials Innovation Research Center, Division of Engineering in Medicine, Brigham and Women's Hospital, Harvard Medical School, Cambridge, MA 02139, USA

Correspondence to: Yu Shrike Zhang; Ali Khademhosseini.

[†]These authors contributed equally to this work as the primary author.

Supporting Information

Supporting Information is available online from the Wiley Online Library or from the author.

Harvard-MIT Division of Health Sciences and Technology, Massachusetts Institute of Technology, Cambridge, MA 02139, USA

Syeda Mahwish Bakht,
Biomaterials Innovation Research Center, Division of Engineering in Medicine, Brigham and Women's Hospital, Harvard Medical School, Cambridge, MA 02139, USA

Harvard-MIT Division of Health Sciences and Technology, Massachusetts Institute of Technology, Cambridge, MA 02139, USA

COMSATS Institute of Information and Technology, Islamabad 45550, Pakistan

Prof. Mario Moisés Alvarez,
Biomaterials Innovation Research Center, Division of Engineering in Medicine, Brigham and Women's Hospital, Harvard Medical School, Cambridge, MA 02139, USA

Harvard-MIT Division of Health Sciences and Technology, Massachusetts Institute of Technology, Cambridge, MA 02139, USA

Microsystems Technologies Laboratories, Massachusetts Institute of Technology, Cambridge, MA 02139, USA

Centro de Biotecnología-FEMSA, Tecnológico de Monterrey at Monterrey, Monterrey, Nuevo León, CP 64849, México

Dr. Jingzhou Yang,
Biomaterials Innovation Research Center, Division of Engineering in Medicine, Brigham and Women's Hospital, Harvard Medical School, Cambridge, MA 02139, USA

Harvard-MIT Division of Health Sciences and Technology, Massachusetts Institute of Technology, Cambridge, MA 02139, USA

School of Mechanical and Chemical Engineering, University of Western Australia, Perth, WA 6009, Australia

Dr. Yi-Chen Li,
Biomaterials Innovation Research Center, Division of Engineering in Medicine, Brigham and Women's Hospital, Harvard Medical School, Cambridge, MA 02139, USA

Harvard-MIT Division of Health Sciences and Technology, Massachusetts Institute of Technology, Cambridge, MA 02139, USA

Dr. Grissel Trujillo-de Santiago,
Biomaterials Innovation Research Center, Division of Engineering in Medicine, Brigham and Women's Hospital, Harvard Medical School, Cambridge, MA 02139, USA

Harvard-MIT Division of Health Sciences and Technology, Massachusetts Institute of Technology, Cambridge, MA 02139, USA

Microsystems Technologies Laboratories, Massachusetts Institute of Technology, Cambridge, MA 02139, USA

Centro de Biotecnología-FEMSA, Tecnológico de Monterrey at Monterrey, Monterrey, Nuevo León, CP 64849, México

Dr. Amir K. Miri,
Biomaterials Innovation Research Center, Division of Engineering in Medicine, Brigham and Women's Hospital, Harvard Medical School, Cambridge, MA 02139, USA

Harvard-MIT Division of Health Sciences and Technology, Massachusetts Institute of Technology, Cambridge, MA 02139, USA

Dr. Kai Zhu,
Biomaterials Innovation Research Center, Division of Engineering in Medicine, Brigham and Women's Hospital, Harvard Medical School, Cambridge, MA 02139, USA

Harvard-MIT Division of Health Sciences and Technology, Massachusetts Institute of Technology, Cambridge, MA 02139, USA

Department of Cardiac Surgery, Zhongshan Hospital, Fudan University, Shanghai 200032, P.R. China

Shanghai Institute of Cardiovascular Disease, Shanghai 200032, P.R. China

Dr. Parastoo Khoshakhlagh,
Biomaterials Innovation Research Center, Division of Engineering in Medicine, Brigham and Women's Hospital, Harvard Medical School, Cambridge, MA 02139, USA

Harvard-MIT Division of Health Sciences and Technology, Massachusetts Institute of Technology, Cambridge, MA 02139, USA

Wyss Institute for Biologically Inspired Engineering, Harvard University, Boston, MA 02115, USA

Gyan Prakash,
Biomaterials Innovation Research Center, Division of Engineering in Medicine, Brigham and Women's Hospital, Harvard Medical School, Cambridge, MA 02139, USA

Harvard-MIT Division of Health Sciences and Technology, Massachusetts Institute of Technology, Cambridge, MA 02139, USA

Hao Cheng,
Biomaterials Innovation Research Center, Division of Engineering in Medicine, Brigham and Women's Hospital, Harvard Medical School, Cambridge, MA 02139, USA

Harvard-MIT Division of Health Sciences and Technology, Massachusetts Institute of Technology, Cambridge, MA 02139, USA

Xiaofei Guan,
Biomaterials Innovation Research Center, Division of Engineering in Medicine, Brigham and Women's Hospital, Harvard Medical School, Cambridge, MA 02139, USA

Harvard-MIT Division of Health Sciences and Technology, Massachusetts Institute of Technology, Cambridge, MA 02139, USA

Zhe Zhong,
Biomaterials Innovation Research Center, Division of Engineering in Medicine, Brigham and Women's Hospital, Harvard Medical School, Cambridge, MA 02139, USA

Harvard-MIT Division of Health Sciences and Technology, Massachusetts Institute of Technology, Cambridge, MA 02139, USA

Dr. Jie Ju,
Biomaterials Innovation Research Center, Division of Engineering in Medicine, Brigham and Women's Hospital, Harvard Medical School, Cambridge, MA 02139, USA

Harvard-MIT Division of Health Sciences and Technology, Massachusetts Institute of Technology, Cambridge, MA 02139, USA

Geyunjian Zhu,
Biomaterials Innovation Research Center, Division of Engineering in Medicine, Brigham and Women's Hospital, Harvard Medical School, Cambridge, MA 02139, USA

Harvard-MIT Division of Health Sciences and Technology, Massachusetts Institute of Technology, Cambridge, MA 02139, USA

Department of Polymer Engineering, University of Akron, 200E Exc 160, Akron, OH 44304, USA

Prof. Xiangyu Jin,
Key Laboratory of Textile Science and Technology, College of Textiles, Donghua University, Shanghai 201620, China

Dr. Su Ryon Shin,
Biomaterials Innovation Research Center, Division of Engineering in Medicine, Brigham and Women's Hospital, Harvard Medical School, Cambridge, MA 02139, USA

Harvard-MIT Division of Health Sciences and Technology, Massachusetts Institute of Technology, Cambridge, MA 02139, USA

Wyss Institute for Biologically Inspired Engineering, Harvard University, Boston, MA 02115, USA

Prof. Mehmet Remzi Dokmeci, and
Biomaterials Innovation Research Center, Division of Engineering in Medicine, Brigham and Women's Hospital, Harvard Medical School, Cambridge, MA 02139, USA

Harvard-MIT Division of Health Sciences and Technology, Massachusetts Institute of Technology, Cambridge, MA 02139, USA

Wyss Institute for Biologically Inspired Engineering, Harvard University, Boston, MA 02115, USA

Prof. Ali Khademhosseini
Biomaterials Innovation Research Center, Division of Engineering in Medicine, Brigham and Women's Hospital, Harvard Medical School, Cambridge, MA 02139, USA

Harvard-MIT Division of Health Sciences and Technology, Massachusetts Institute of Technology, Cambridge, MA 02139, USA

Wyss Institute for Biologically Inspired Engineering, Harvard University, Boston, MA 02115, USA

Department of Bioindustrial Technologies, College of Animal Bioscience and Technology, Konkuk University, Seoul 143-701, Republic of Korea

Department of Physics, King Abdulaziz University, Jeddah 21569, Saudi Arabia

Keywords

Bioprinting; multi-material; hydrogel; bioink; tissue engineering

Recent advancements in bioprinting technologies have significantly improved our capability to fabricate artificial tissues and biomedical devices through bottom-up assembly of biomaterials, biomolecules, and cells.[1] The spatial arrangement of distinctive components in the resulting constructs is of critical importance to achieve tissue and device functions. The bioprinting technologies, including extrusion-based printing,[2] laser-based printing,[3] inkjet-based printing,[4] acoustic encapsulation,[5] and valve-based printing,[6, 7] have provided robust platforms that allow for controlled deposition of three-dimensional (3D) constructs with pre-defined patterns. Among these different methods, extrusion-based bioprinting is one of the most popular methodologies presently used due to its compatibility with various bioinks and ease of operation.[8]

A typical extrusion bioprinter is composed of three units: a reservoir (*e.g.,* syringe) that contains the bioink, a printhead through which the bioink is ejected from the reservoir, and a receiving stage where the deposited bioink is collected.[9] The printhead, the stage, or both, may be motorized to achieve elaborate control of bioprinting based on precisely designed patterns. Nevertheless, most of the current modalities are limited to the use of a single bioink during each deposition process, rendering it difficult to achieve bioprinting of sophisticated compositional structures. Several techniques have recently been advanced to overcome this limitation in an effort to improve the capacity of bioprinters to extrude more than a single bioink. For example, a simple mixing device was fixed onto the printhead for printing of two materials.[10–12] In addition, multi-material bioprinting was realized by incorporating multiple separate printheads on a bioprinter, where mechanical co-registration of the printheads achieved the deposition of selected inks at desired locations.[13, 14, 15, 16] Despite their potential in scaling up to a larger number of materials, the deposition speed of this technique would inevitably be reduced as more nozzles are added, since fast switching among different channels and simultaneous injection of bioinks can hardly be achieved.

Here, we report a multi-material extrusion bioprinting platform that is capable of extruding multiple coded bioinks in a continuous manner with fast and smooth switching among different reservoirs for rapid fabrication of complex (tissue) constructs. This paper provides a proof-of-concept demonstration by mounting a single printhead consisting of a bundle of 7 equal-sized capillaries, each connected to a unique bioink reservoir that could be individually actuated by digitally controlled pneumatic pressure. The ejection process, when synergized with the movement of the motorized stage, allows for rapid deposition of two-dimensional (2D) patterns and 3D architectures composed of multiple desired bioinks in a spatially defined manner, at a speed an order of magnitude faster than most existing nozzle-based bioprinting modalities. We further demonstrated the capability of our rapid continuous multi-material bioprinter to generate miniaturized cell-laden constructs containing several types of cells, as well as its potential to fabricate gradient structures, and prototype multi-component bioelectronics, using a broad range of bioinks derived from shear-thinning to conductive biomaterials. The proposed technology is likely to advance the field of extrusion

bioprinting by offering strong capacity in printing speed and continuity, which is compatible with a wide variety of bioinks. Most of all, our 3D bioprinting platform may be conveniently extended to a large numbers of bioinks necessary for engineering highly complex functional biomaterials, tissues, and devices in the future.

Unlike conventional multi-nozzle bioprinters, which typically require mechanical switching among the physically separated nozzles to deposit multiple bioinks, our bioprinter is able to continuously eject different types of bioinks in both individual and simultaneous modes. The bioprinter consists of a Cartesian robotic stage and an array of bioink reservoirs routed to a single printhead containing 7 bundled channels with equal sizes (Figure 1, A–D, Figures S1 and S2). The dispensers are pneumatically driven and fed by compressed gas through valves (Figure 1C). Digital tuning of the extrusion is achieved using a program integrated with the bioprinter to individually (or simultaneously) switch on/off desired valve(s) and command the dispensing patterns (Figure 1, B and C). The controllers for both the valves and the motorized stage are programmed to synchronize the actuation of the valves and the movement of the stage. The adjustment of the pneumatic pressure and valve gating duration allows the dispersion of various bioinks with different viscosities. As such, this bioprinter can print up to 7 materials and rapidly switch among materials from different channels, without needing to physically change the nozzles.

Here a shear-thinning bioink formulated by a suspension of synthetic nanosilicates in water was employed for bioprinting.[17, 18] Detailed investigations of the rheological properties and the printing performance of silicate bioink can be found in Supporting Information (Figures S3–S6). It should be noted that the 5% nanosilicate bioink was chosen as the optimal formulation that possessed proper shear-thinning properties, and was thus used to bioprint various 3D constructs. As an example, we programed the bioprinter to deposit bioinks dyed in 7 different colors with increasing numbers of colors after each switch (Figure 1, E and F, and movie S1). The bioprinting process was continuous, and the printed microfibrous structure maintained its three-dimensionality consisting of an array of spatially well-defined bioinks (Figure 1G). The 7 bioinks could also be individually deposited *via* a continuous printing process (movie S2), where no noticeable switching delays were observed between adjacent materials (Figure S7).

We next printed a series of microfibrous 2D patterns to demonstrate the capability of our bioprinter for continuous extrusion of multiple materials in well-defined manners. Each of the 7 bioinks could be continuously printed in equivalent lengths along the direction of the individual microfibers, with equal or incremental spacing between the adjacent lines (Figure S8, A and B). Alternatively, the spacing between the adjacent microfibers could be maintained constant while continuous segments within individual lines were printed with decreasing lengths (Figure S8C), or both parameters might be altered simultaneously during the bioprinting process (Figure S8D). We further printed an array of microfibers composed of increments of 1–7 materials along the direction of individual lines (Figure S8E). Printing of these various patterns demonstrated the capability of our platform to continuously deposit any desired type and number of bioinks on demand. The different materials could also be printed in perpendicular directions, to achieve hierarchical architecture while still maintaining a clear separation of the deposited bioinks (Figure S8, F–J). The printed multi-

material microfibers could be designed to fuse into a single piece of structure when the spacing between the microfibers was reduced to match their width (movie S3). The printed microfibers joined each other and formed a cohesive piece of monolayer slab containing 7 distinct but continuous segments along the direction of microfiber deposition. This ability to create fused larger-scale constructs allowed us to print more sophisticated patterns composed of multiple bioinks, which has hardly been possible using existing multi-printhead systems.[13] Our continuous multi-material bioprinter has shown unparalleled power in overcoming this inability by depositing multiple types of materials in precisely programmed arrangements at much improved fabrication speed.

It is estimated that our continuous multi-material bioprinter features much faster fabrication speed than most existing multi-nozzle systems. For a typical multi-nozzle printer, the switch time between nozzles averages 4–20 s.[14, 16] In comparison, our continuous bioprinting platform requires nearly no gap in such switching processes. In analyzing our fabrication procedure where we printed 15 lines each composed of 7 bioinks for 2 layers (and thus 180 switches in total, movie S3), while our continuous bioprinter spent only 256 s for the entire printing process (at a speed of 400 mm min^{-1}), a conventional multi-nozzle printer will consume an additional time of 720–3600 s simply devoted to physical nozzle switching and result in a total printing time of 976–3856 s, if the patterns are deposited in the same manner. Therefore, our continuous multi-material bioprinter could achieve a speed up to 15 times faster than those of the existing nozzle-based platforms. Although the numbers in this comparison is not completely accurate due to the different materials used in the literature and in our case, it is still indicative of the potential superior capacity of our multi-material bioprinter to deposit several bioinks than existing multi-nozzle platforms. The advantage of our continuous multi-material extrusion printing system in terms of the biofabrication speed would become much more pronounced as the number of materials and the complexity of the printouts are increased. These unique features of our bioprinter have significantly promoted the current level of automation and speed among existing nozzle-based bioprinting techniques.[11, 14, 19] It should be noted that, the present system is readily expandable to as many bioinks as needed by simply increasing the number of pneumatically driven valves and reservoirs, thus affording us the possibility to rapidly generate complex constructs while simplifying instrumentation.

We next demonstrated the capability of our continuous multi-material bioprinter to produce complex 3D constructs. Simple cubes composed of 2 and 3 bioinks (Figure 2, A and B) and ring-shaped blocks containing 2, 3, and 4 bioinks were readily printed (Figure 2, C–E). Constructs containing all 7 bioinks could also be fabricated in different shapes, such as a pyramid (Figure 2F), a three-layer stripe (Figure 2G), and a ten-layer stripe (Figure 2H). We further designed sophisticated 3D patterns and printed a set of structures resembling human organs, including brain, lung, heart, liver, kidneys, pancreas, gastrointestinal system, and bladder. Each organ-like structure contained 4–7 bioinks, according to the requirements of local structures, and each was individually printed (Figure 2I and movies S4–S7). Only 1–3 layers of the bioinks were deposited in these examples due to the significant amount of time required for printing these structures of relatively large scales. The bioprinting processes were rapid, and the transition among different bioinks was smooth. The printed organ-like constructs were stable, and the demarcation among adjacent materials was clear (Figures 2,

J–N, and S9). Our multi-material bioprinter was also compatible with the embedded bioprinting technique.[7] Using a modified printhead with extended length, we were able to directly generate free-form shape of polyethylene glycol-diacrylate (PEGDA)/alginate coils in a pluronic hydrogel followed by photocrosslinking and retrieval after liquefying the supporting matrix (Figure 2O). Similarly, free-form alginate shapes composed of multiple bioinks, such as a dual-layer hollow tube (Figure 2P) and a DNA double helix (Figure 2Q), could be obtained with our continuous multi-material bioprinter.

The developed rapid continuous multi-material bioprinter should be able to generate hierarchical structures and patterns suitable for various applications in biomedicine. We subsequently demonstrated the capability of the bioprinter in engineering complex cell-laden organs and depositing prototype bioelectronic circuits. While these demonstrations are preliminary with limited resolution and functional assays, we primarily aimed to validate the concept of our continuous multi-material extrusion bioprinting in the current work.

Among the various photocrosslinkable hydrogels available, gelatin methacryloyl (GelMA) has been frequently used as a bioink due to its intrinsic cell adhesion moieties that promote cell spreading and functionality.[20] Here, we adopted a mixture of GelMA and alginate as the bioink,[10] where the alginate component was used to increase the viscosity to achieve a range of bioprinting conditions. The cell-laden bioinks were photocrosslinked to fix their structures immediately after printing.[10] Detailed investigations of the rheological properties and the printing performance of the GelMA/alginate bioinks can be found in Supporting Information (Figures S10–S12). We first took advantage of the multi-bioink printing to design a range of different patterns including a heart-like structure (Figure 3, A–E), a kidney-like structure (Figure S13, A–F), and stripes with different width (Figure S13, G–K). It was clear that, multiple bioinks laden with cells pre-labeled with cell trackers were effectively deposited using our continuous multi-material bioprinter. The printed structure possessed explicitly separated borders among different cell-laden bioinks (Figures 3, B–E, and S13 B–F, and H–K). The resolution was determined to be approximately 100–200 μm, as indicated from the printed stripe patterns with a range of widths (Figure S13, H–K).

We further printed a pattern of endotheliaized tissue, where four sectors of bioinks laden with human dermal fibroblasts (HDFs), human hepatocellular cells (HepG2), human mesenchymal stem cells (hMSCs), and no cells, respectively, were deposited at the base, followed by integration of a pattern on top that resembled the vasculature encapsulating human umbilical vein endothelial cells (HUVECs, Figure 3F). The fluorescence micrographs obtained from different locations clearly revealed successful bioprinting of the desired (cell-laden) bioinks (Figure 3, G–I), which laid down the essential basis for future fabrication of complex tissues containing hierarchical assembly of multiple cell types. The cell viability assays, determined immediately and at 1 and 7 days post bioprinting (Figures 3J and S14, A–T), indicated that all cell types maintained sufficient viability under the UV crosslinking conditions adopted. Comparison with the cells pre-bioprinting (Figure S14, A–H *versus* I–T) further revealed that the conditions selected for extrusion did not appear to affect cell viability. The cells well spread over a course of 7 days in culture (Figure S14, U–X), indicating the bioactivity provided by the GelMA component of the bioink. The printed

vascularized tissue constructs were further shown to exhibit increased cell proliferation over a period of 3 days analyzed (Figure 3K).

In addition, we used the multi-material extrusion bioprinter to generate gradient structures to mimic those occurring in natural tissues, such as the bone. For example, we created a ring-like structure featuring an inward-out gradient in the concentration of hydroxyapatite (HAp) embedded in the GelMA/alginate hydrogel (Figure 4A). Alizarin Red staining and quantification of the staining intensities further confirmed the presence of this same type of gradient in HAp contents (Figure 4, B and C). Importantly, the shape of the printed constructs containing bioinks with different concentrations of HAp could be arbitrarily controlled to form any desired localized gradients as well as continuous or discrete patterns, as illustrated by our capability to print a bone-shaped hydrogel block (Figure 4D). The Alizarin Red staining indicated that different bioinks containing a range of HAp concentrations were printed across the entire structure, where the same materials (#4 and 5, #6 and 7) printed at discrete locations showed similar staining intensity, revealing reproducible deposition of the bioinks as programmed (Figure 4E).

The printed constructs featuring gradients of inorganic nanoparticles also demonstrated varying bioactivities. Differential attachment and proliferation of MC3T3 preosteoblasts seeded on top of the printed structure containing a gradient of HAp, were observed after 1 and 3 days of culture (Figure 4, F and H). The cell seeding efficiency and proliferation were promoted with increasing concentration of HAp. A similar trend in cell behaviors was observed when the preosteoblasts were seeded on printed hydrogels containing a gradient of nanosilicates based on the osteoinductive property of these nanoparticles (Figure 4, G and I).[18] This excellent freedom in reliable and smooth switching among selected bioinks during the bioprinting process is critical in recapitulating tissue- and organ-level biomimetic properties, especially when sophisticated structures and/or complex compositions are involved.

Significant interest in bioelectronics is also emerging in biomedicine. A wide range of applications of electronics devices is possible in various fields, including epidermal sensors, soft contact lenses, neurointerfaces, implantable medical devices, and bioactuators.[21] Bioprinting has been increasingly recognized as an excellent technique for depositing conductive bioinks for direct fabrication of bioelectronics, given its convenience, robustness, and cost effectiveness.[22] While many strategies have been developed for printing conductive bioinks, these have been mostly limited by single-ink deposition, which precluded the possibility for the production of complex electronic circuits. Taking advantage of our multi-material bioprinting platform, we printed a prototype continuous circuit featuring conductive alginate/DNA/carbon nanotube (CNT) bioinks with 1–6 mg mL^{-1} CNTs in parallel (Figure 4, J and K, and movie S8). This conductive bioink was optimized from our previous formulation used for single-material printing.[23] The printed circuit was completed by attaching a power source (coin battery, 3V) and 6 miniature green LEDs, which upon connection, exhibited a clear gradient in their luminescence intensity (Figure 4L). The differential luminescence of the LEDs was attributed to the series of resistances (0.17–3.37 Ω mm^{-1}) that the conductive bioinks produced and therefore the difference in the current generated in each parallel unit (Figure 4, M and N). Our capability for continuously

printing several types of conductive bioinks has paved a new avenue for fabricating complex bioelectronics, where future bioprinting of complex circuits composed of multiple functional electronic units is envisioned.

In summary, we have developed a continuous multi-material extrusion bioprinting strategy capable of continuously and/or simultaneously depositing up to 7 types of bioinks through the integration of a digitally tunable pneumatic single-printhead system, which was able to achieve biofabrication of multi-component structures at a speed up to 15 times faster than existing nozzle-based modalities. While our demonstrations in the current work are preliminary with limited resolution and functional assays, we primarily aimed to introduce the concept of continuous multi-material extrusion bioprinting. To this end, we demonstrated the capacity of this platform in bioprinting of sophisticated planar and 3D patterns. In the subsequent proof-of-concept demonstrations, we showed the ability of our bioprinter to produce complex and gradient constructs for applications in tissue engineering, point-of-care diagnosis, and bioelectronics. Notably, our platform may be readily expanded to a large number of channels desired, simply by increasing the numbers of digitally actuated pneumatic valves in the system.

We believe that further optimization in the instrumentation of the bioprinting system will make it a highly efficient modality and a leap forward in the fabrication of physiologically relevant and functional tissues/organs that match the complexity of their *in vivo* counterparts at clinically relevant speeds. For example, it should be noted that, in the current setup we aligned the individual channels of the printhead side by side, leading to slightly non-concentric deposition of the multiple bioinks. Nonetheless, the printhead could be further connected to a common outlet, and this different printhead design enabling the materials to mix with different volumes/rates prior to extrusion would further achieve true gradient formation at microscale. The pressure of each channel may also be individually tuned (as to the uniform pressures across different channels in our current system) to allow for dispensing of multiple bioinks with a series of rheological properties. Further optimization of the bioprinter is currently undergoing and will be reported in future publications. We foresee the widespread use of our multi-material extrusion bioprinting in rapid construction of biomedical devices where a multitude of different materials can be adapted.

Supplementary Material

Refer to Web version on PubMed Central for supplementary material.

Acknowledgments

The authors acknowledge funding from the National Institutes of Health (AR057837, DE021468, D005865, AR068258, AR066193, EB022403, EB021148), and the Office of Naval Research Presidential Early Career Award for Scientists and Engineers (PECASE). Y. S. Zhang acknowledges the National Cancer Institute of the National Institutes of Health Pathway to Independence Award (1K99CA201603-01A1). This work was also partially supported by the Fundamental Research Funds for the Central Universities from China (No. 14D310106). W. Liu further appreciates the financial support from the program of China Scholarships Council (No. 201406630041). We thank E. Laukaitis for her assistance with the schematic diagram in Figure 1A. We also thank R. Steinmeyer, R. Lee, and V. Seksaria for their assistance in hardware/software designs of the printer.

References

1. Bajaj P, Schweller RM, Khademhosseini A, West JL, Bashir R. Annual review of biomedical engineering. 2014; 16:247.Malda J, Visser J, Melchels FP, Jüngst T, Hennink WE, Dhert WJ, Groll J, Hutmacher DW. Adv Mater. 2013; 25:5011. [PubMed: 24038336] Murphy SV, Atala A. Nat. Biotechnol. 2014; 32:773. [PubMed: 25093879] Pati F, Jang J, Ha D-H, Kim SW, Rhie J-W, Shim J-H, Kim D-H, Cho D-W. Nature communications. 2014; 5:3935.Stanton MM, Samitier J, Sánchez S. Lab Chip. 2015; 15:3111. [PubMed: 26066320] Zhang YS, Duchamp M, Oklu R, Ellisen LW, Langer R, Khademhosseini A. ACS Biomater Sci Eng. 2016Zhang YS, Yue K, Aleman J, Moghaddam K, Bakht SM, Dell'Erba V, Assawes P, Shin SR, Dokmeci MR, Oklu R, Khademhosseini A. Ann. Biomed. Eng. 2016
2. Yan Y, Wang X, Pan Y, Liu H, Cheng J, Xiong Z, Lin F, Wu R, Zhang R, Lu Q. Biomaterials. 2005; 26:5864. [PubMed: 15949552]
3. Nahmias Y, Schwartz RE, Verfaillie C, Odde DJ. Biotechnology and bioengineering. 2005; 92:129. [PubMed: 16025535]
4. Nakamura M, Kobayashi A, Takagi F, Watanabe A, Hiruma Y, Ohuchi K, Iwasaki Y, Horie M, Morita I, Takatani S. Tissue Eng. 2005; 11:1658. [PubMed: 16411811]
5. Demirci U, Montesano G. Lab on a chip. 2007; 7:1139. [PubMed: 17713612]
6. Demirci U, Montesano G. Lab on a chip. 2007; 7:1428. [PubMed: 17960267] Miller JS, Stevens KR, Yang MT, Baker BM, Nguyen D-HT, Cohen DM, Toro E, Chen AA, Galie PA, Yu X. Nat. Mater. 2012; 11:768. [PubMed: 22751181]
7. Bhattacharjee T, Zehnder SM, Rowe KG, Jain S, Nixon RM, Sawyer WG, Angelini TE. Science Adv. 2015; 1:e1500655.Highley CB, Rodell CB, Burdick JA. Adv. Mater. 2015; 27:5075. [PubMed: 26177925] Hinton TJ, Jallerat Q, Palchesko RN, Park JH, Grodzicki MS, Shue H-J, Ramadan MH, Hudson AR, Feinberg AW. Science Adv. 2015; 1:e1500758.
8. Jones N. Nature. 2012; 487:22. [PubMed: 22763531]
9. Seol Y-J, Kang H-W, Lee SJ, Atala A, Yoo JJ. European Journal of Cardio-Thoracic Surgery. 2014:ezu148.
10. Colosi C, Shin SR, Manoharan V, Massa S, Constantini M, Barbetta A, Dokmeci MR, Dentini M, Khademhosseini A. Adv. Mater. 2015; 28:677. [PubMed: 26606883]
11. Hardin JO, Ober TJ, Valentine AD, Lewis JA. Adv. Mater. 2015; 27:3279. [PubMed: 25885762]
12. Ober TJ, Foresti D, Lewis JA. Proct. Natl. Acad. Sci. U.S.A. 2015; 112:12293.
13. Chang R, Nam J, Sun W. Tissue Eng. A. 2008; 14:41.Khalil S, Nam J, Sun W. Rapid Prototyping Journal. 2005; 11:9.Yu Z, Rui Y, Liliang O, Hongxu D, Ting Z, Kaitai Z, Shujun C, Wei S. Biofabrication. 2014; 6:035001. [PubMed: 24722236]
14. Kolesky DB, Truby RL, Gladman AS, Busbee TA, Homan KA, Lewis JA. Adv. Mater. 2014; 26:3124. [PubMed: 24550124]
15. Campbell J, McGuinness I, Wirz H, Sharon A, Sauer-Budge AF. Journal of Nanotechnology in Engineering and Medicine. 2015; 6:021005.Merceron TK, Burt M, Seol Y-J, Kang H-W, Lee SJ, Yoo JJ, Atala A. Biofabrication. 2015; 7:035003. [PubMed: 26081669]
16. Kang H-W, Lee SJ, Ko IK, Kengla C, Yoo JJ, Atala A. Nat. Biotechnol. 2016; 34:312. [PubMed: 26878319]
17. Gaharwar AK, Avery RK, Assmann A, Paul A, McKinley GH, Khademhosseini A, Olsen BD. ACS Nano. 2014; 8:9833. [PubMed: 25221894] Ruzicka B, Zaccarelli E. Soft Matter. 2011; 7:1268.
18. Gaharwar AK, Mihaila SM, Swami A, Patel A, Sant S, Reis RL, Marques AP, Gomes ME, Khademhosseini A. Adv Mater. 2013; 25:3329. [PubMed: 23670944]
19. Bertassoni LE, Cardoso JC, Manoharan V, Cristino AL, Bhise NS, Araujo WA, Zorlutuna P, Vrana NE, Ghaemmaghami AM, Dokmeci MR. Biofabrication. 2014; 6:024105. [PubMed: 24695367]
20. Nichol JW, Koshy ST, Bae H, Hwang CM, Yamanlar S, Khademhosseini A. Biomaterials. 2010; 31:5536. [PubMed: 20417964] Yue K, Santiago G Trujillo-de, Alvarez MM, Tamayol A, Annabi N, Khademhosseini A. Biomaterials. 2015; 73:254. [PubMed: 26414409]

21. Gaikwad AM, Whiting GL, Steingart DA, Arias AC. Adv Mater. 2011; 23:3251. [PubMed: 21661062] Kim, Dae-Hyeong; Lu, Nanshu; Ghaffari, Roozbeh; Rogers, JA. NPG Asia Materials. 2012; 4:15.Garnier F, Hajlaoui R, Yassar A, Srivastava P. Science. 1994; 265:1684. [PubMed: 17770896] Duan X, Fu TM, Liu J, Lieber CM. Nano Today. 2013; 8:351. [PubMed: 24073014]

22. Muth JT, Vogt DM, Truby RL, Menguc Y, Kolesky DB, Wood RJ, Lewis JA. Advanced Materials. 2014; 26:6307. [PubMed: 24934143] Secor EB, Lim S, Zhang H, Frisbie CD, Francis LF, Hersam MC. Advanced Materials. 2014; 26:4533. [PubMed: 24782064]

23. Shin SR, Farzad R, Tamayol A, Manoharan V, Mostafalu P, Zhang YS, Akbari M, Jung SM, Kim D, Commotto M, Annabi N, Al-Hazmi FE, Dokmeci MR, Khademhosseini A. Adv. Mater. 2016; 28:3280. [PubMed: 26915715]

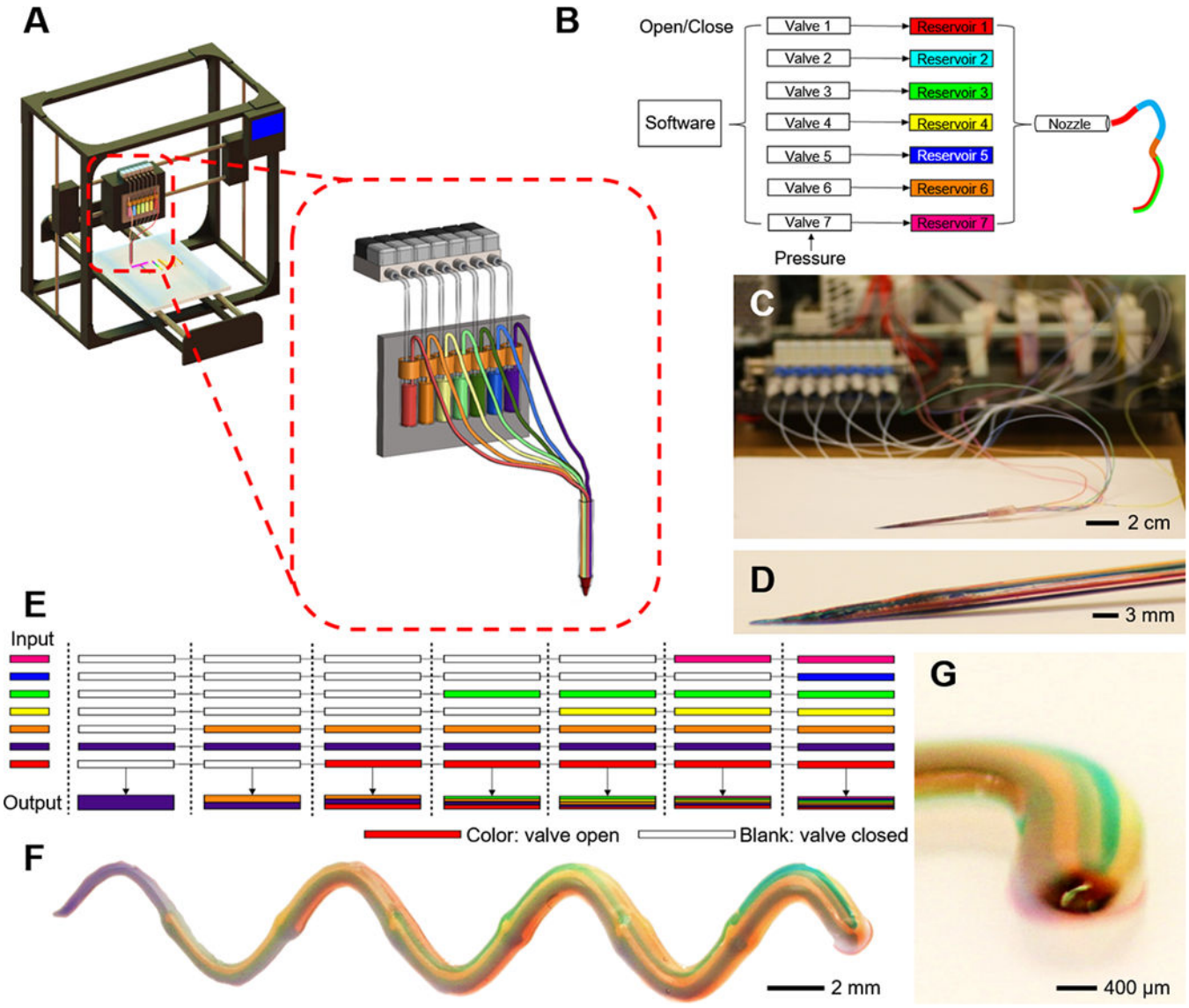

Figure 1. Design of the digitally tunable continuous multi-material extrusion bioprinter

(A and B) Schematics showing the design of the 7-channel printhead connected to reservoirs that are individually actuated by programmable pneumatic valves. (C and D), Photographs showing the setup of the Festo valves and printhead. (E) Schematic of a sample code for continuous bioprinting of a single serpentine microfiber consisting of 1–7 bioinks. (F) Photograph showing the printed microfiber. (G) Side view of the end of the microfiber indicating the 3D volume containing 7 individually segmented bioinks. Printing conditions: 5% nanosilicate aqueous suspension dyed in 7 different colors, printhead moving speed = 400 mm min−1, pneumatic pressure = 50 psi.

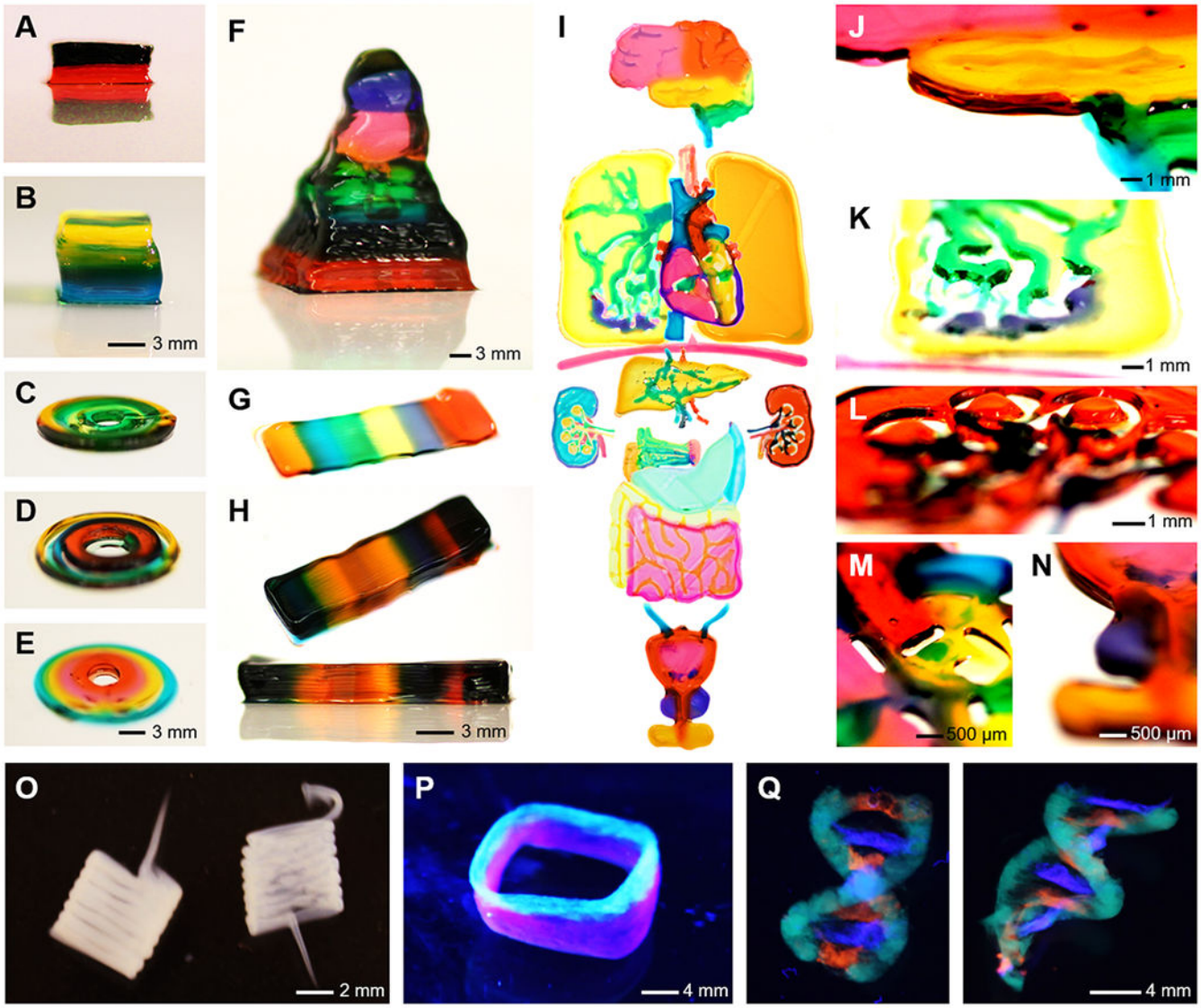

Figure 2. Multi-material bioprinting of 3D constructs

(A and B) Bioprinting of dual- and triple-layered cuboid blocks. (C–E) Bioprinting of blood vessel-like structures (transverse plane) containing dual, triple, and quadruple materials. (F) Bioprinting of a pyramid containing 7 layers of different bioinks. (G and H) Bioprinting of 3 and 10-layered blocks with continuous segments of 7 different bioinks. (I) Bioprinting of human organ-like constructs from multiple bioinks, including brain, lung, heart, liver, kidneys, pancreas, stomach, small/large intestines, bladder, and prostate. The organ-like constructs were individually printed, photographed, and stitched together in the same image at relative locations as those in the human body. (J–N) Side view of selected organ-like constructs indicating their 3D nature: (J) brain, (K) lung vasculature, (L) kidney, (M) left atrium of heart, (N) bladder/prostate. The organ-like structures were not printed to scale to each other. (A–N) printing conditions: 5% nanosilicate aqueous suspension dyed in 7 different colors, printhead moving speed = 400 mm min^{-1}, pneumatic pressure = 50 psi. (O–Q) embedded bioprinting of free-form (O) coils (printing conditions: 20% PEGDA, 2%

alginate, and 0.5% PI extruded in 23% Pluronic aqueous solution; printhead moving speed = 100 mm min^{-1}, pneumatic pressue = 30 psi), (P) dual-layer hollow tube, and (Q) DNA helix in front and side views. (P and Q) printing conditions: 2% alginate dyed in different colors extruded in 23% Pluronic aqueous solution containing 0.05% $CaCl_2$; printhead moving speed = 100 mm min^{-1}, pneumatic pressue = 30 psi.

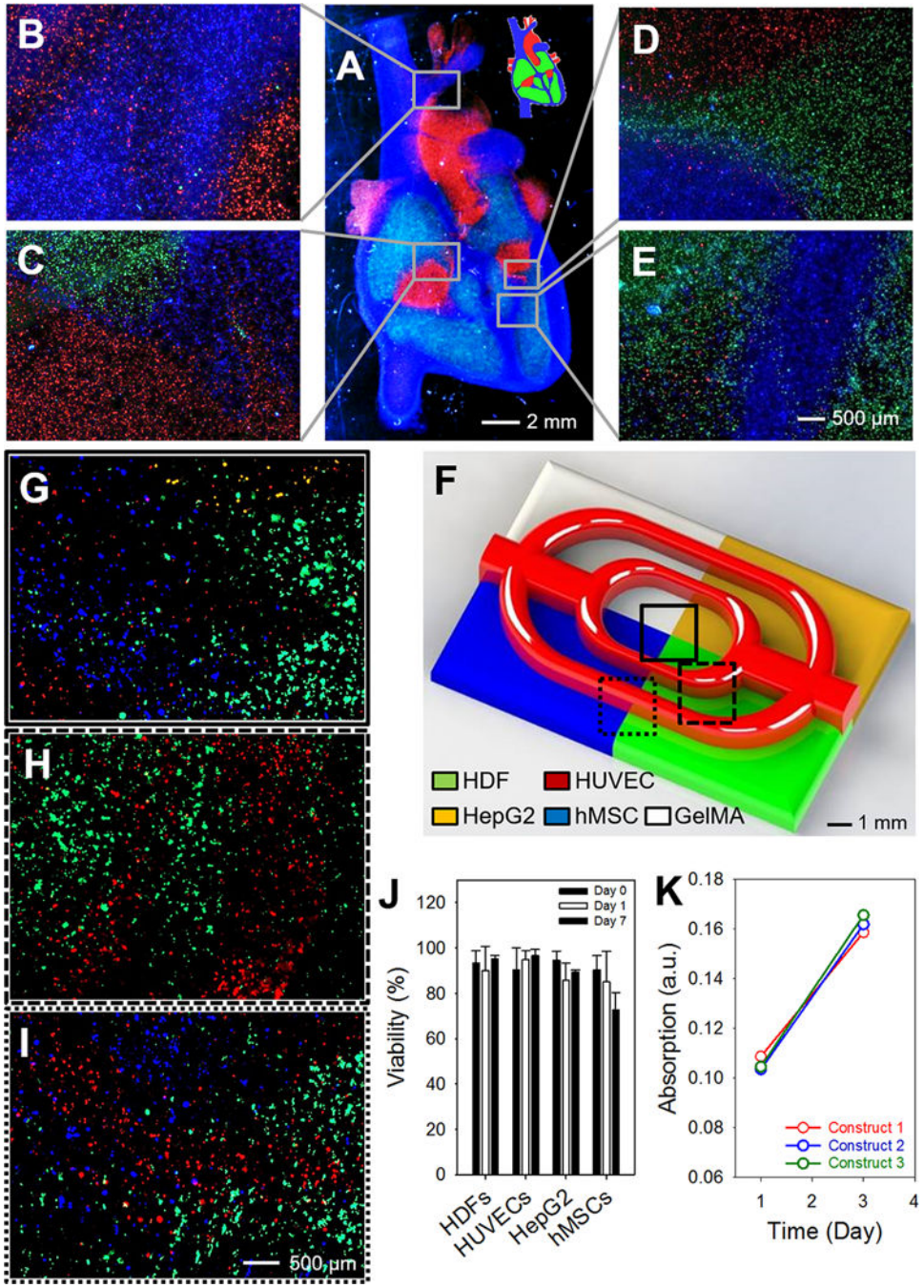

Figure 3. Multi-material bioprinting of cell-laden structures

(A) Fluorescence image showing a printed multi-component heart-like structure. Fluorescent microbeads were used to aid the macroscopic visualization. The inset shows a schematic of the design. (B–E) Fluorescence micrographs of different junction regions showing the co-existence of HDFs stained with different cell trackers in the printed cell-embedding construct. (F) Schematic showing the design of a vascularized tissue construct containing the four types of cells stained with different cell trackers. (G–I) Fluorescence micrographs of different junction regions showing the co-existence of desired cell types in the printed

construct. (J) Quantification of viability of the four cell types immediately, 1 and 7 days post bioprinting. (K) Proliferation of the cells over a course of 3 days. Printing conditions: 5% GelMA and 1% alginate encapsulating different cells, printhead moving speed = 400 mm min^{-1}, pneumatic pressure = 3 psi.

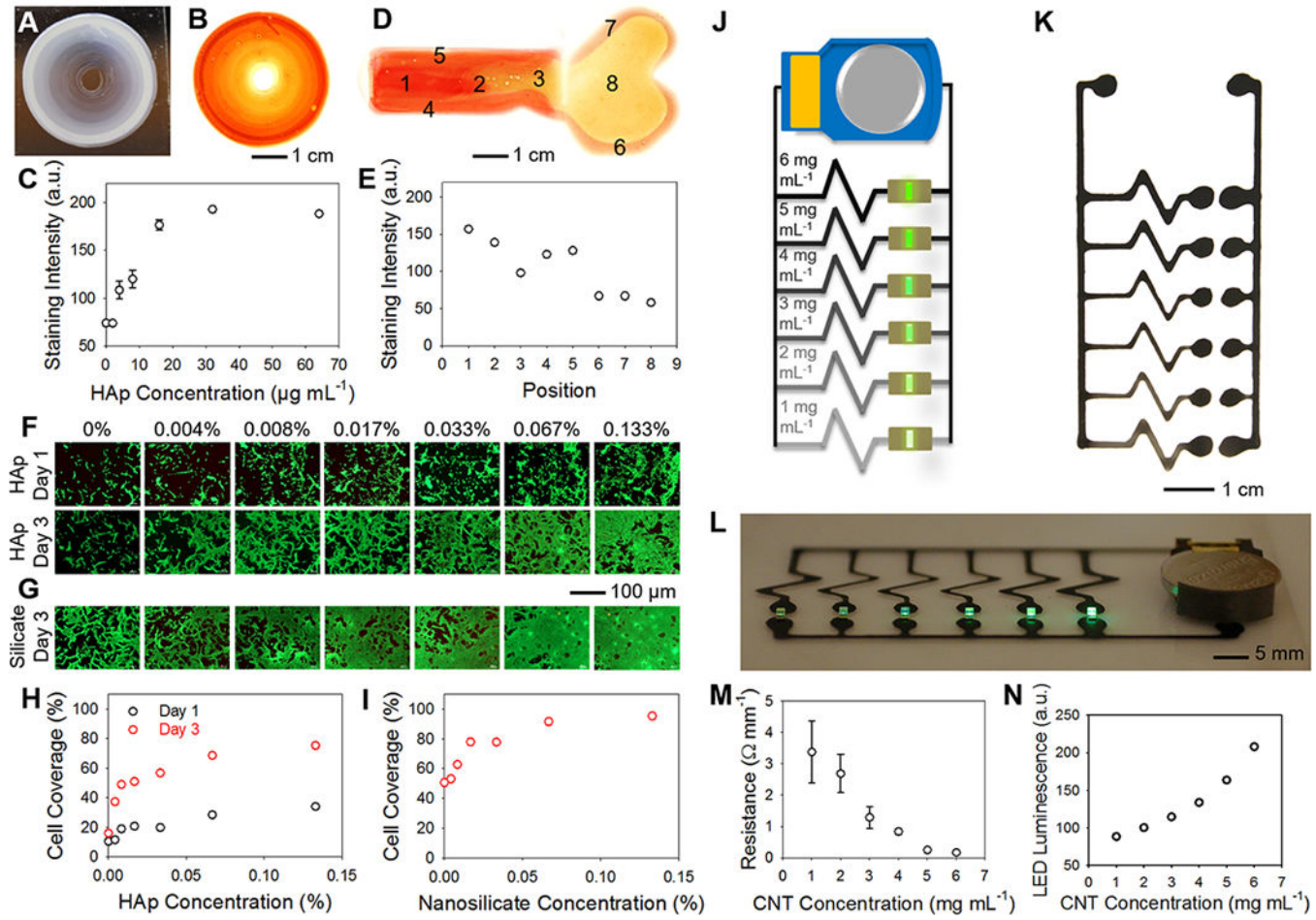

Figure 4. Extended applications of the continuous multi-material bioprinting platform

(A) Printed concentric hydrogel structures containing inward-out gradient of HAp. (B) Alizarin Red staining of the same construct revealing the gradient in HAp contents. (C) Quantification of the Alizarin Red staining intensities for each ring. (D) Printed bone-like structure with desired bioinks containing different concentrations of HAp post staining with Alizarin Red. (E) Quantification of the Alizarin Red staining intensities at selected locations. (F and G) Fluorescence micrograph showing the spreading of preosteoblasts on printed hydrogel blocks with gradients of (F) HAp and (G) nanosilicates. (H and I) Quantifications of area coverages by the cells on the two substrates with HAp and nanosilicate gradients, respectively. Printing conditions: (A to I) 5% GelMA, 2.67% alginate, and 0.5% PI containning various concentrations of HAp and nanosilicates, printhead moving speed = 400 mm min^{-1}, pneumatic pressure = 3 psi. (J) Schematic showing the design of the bioelectronic circuit composed of conductive bioinks with a series concentrations of CNTs. (K) Photograph of a printed circuit. (L) Photograph of a completed circuit where the LEDs showed a series of differential luminescence intensities. (M and N) Quantifications of the resistance and LED luminescence for bioinks containing different concentrations of CNTs. Printing conditions: 2% alginate containning various concentrations of CNTs, printhead moving speed = 400 mm min^{-1}, pneumatic pressure = 3 psi.